Array of plasmonic particles enabling optical near-field concentration: A nonlinear inverse scattering design approach

Arash Rashidi* and Hossein Mosallaei†
Electrical and Computer Engineering Department, Northeastern University, Boston, Massachusetts 02115, USA
(Received 23 December 2009; revised manuscript received 3 March 2010; published 21 July 2010)

The main idea of this paper is to design an array of core-shell plasmonic nanoparticles manipulating a desired near-field focusing pattern in optical spectrum. The interactions between the array elements are formulated by using dyadic Green's function analysis and by employing the closed-form formula for electric polarizability of each plasmonic particle (dipolar mode approach). The point-matching technique is applied to optimize the plasmonic-array field performance as close as to the desired near-field pattern. The final equation for finding the polarizability of each element will be a system of nonlinear equations that can be solved successfully by Levenberg-Marquardt technique. Controlling the inner and outer radii of each element using magnitude and phase contours of polarizability demonstrates a near-field subwavelength concentration. The accuracy of our theoretical model is successfully compared with a full-wave numerical analysis using CST commercial software. Interesting physical features for the optical near-field engineering are illustrated.

DOI: 10.1103/PhysRevB.82.035117 PACS number(s): 42.25.Bs, 78.20.Bh

I. INTRODUCTION

Tightly localizing light and subwavelength near-field focusing are well-understood topics in recent theoretical and experimental optics.[1,2] The major physical obstacle for confining the light in very small spots is the diffraction limit, in which there is a considerable attenuation in evanescent waves for the finer spatial details (smaller than a wavelength).[3] Super-resolution aperture scanning microscope was successful but expensive in fabricating a small aperture in a thin diaphragm to obtain information about the small details features.[4] Theoretically, it can be shown that in a medium of negative index property, evanescent waves can be enhanced in amplitude by perfect lens realization and its unique transmission process.[5] One *L-C* loaded left-handed transmission line medium sandwiched between two commensurate unloaded printed grids experimentally demonstrated the superlens phenomenon[3,6] but the low inductor quality factor is the primary cause of the loss degrading the performance considerably. Some efforts were done recently to theoretically design a near-field focusing plates by back-propagation of the desired near field and then solving an integral equation to find the passive surface impedance.[7,8] One corrugated near-field plate theoretically prompted a subwavelength focal pattern with a null-to-null beamwidth of $\lambda/10$.[9] Another approach has been based on synthesizing the focused pattern by displaced slot elements which enable spatially shifted beams in the near field.[10] The desired weighted magnetic current for each slot is realized by finding the slot dimensions in optimized iteratively full-wave simulations. However, the focus in all of these approaches has been in microwave spectrum where the metal acts like a high-conductivity structure.

The main question is to how manipulate the waves in terahertz spectrum and provide subwavelength near-field focusing in optical region. Notice that, in this frequency spectrum, the metals have dispersion properties with negative permittivity parameters and one would need to take this property into the account for a novel optical concentrator design. Recently, there have been some efforts to shape the light beams in nanometer scale providing far-field directive emission, with the use of optical Yagi-Uda plasmonic nanoantennas (functioning based on the resonant plasmonic core-shell particles),[11] or in more general forms explored in Refs. 12 and 13.

In this paper, we will use the same strategy but for shaping the light in the near-field region establishing a narrow-beamwidth pattern in the focal plane. Our formulation has this capability that we can obtain any two-dimensional subwavelength focusing function as the preferred near-field pattern. Such array of plasmonic particles can be exploited as an array of optical nanoantennas manipulating the waves in the near-field region. The geometry of each concentric core-shell spherical particle, the inner and outer radii, can be tailored for the application of interest. Instead of using time-consuming and convoluted iteratively full-wave simulation to design the inner and outer radii of each element, here we introduce an analytical work based on the dipolar mode analysis and finding the intersection of the amplitude and phase contours for the polarizability in a plane created by two independent variables, the radii ratio (a/b) and the normalized shell radius (b/λ) of the nanoparticles. The other point in our paper is that we will find the dipole mode polarization for each element in an inverse scattering problem (ISP), in which one attempts to infer the properties of the scatterer from the scattered field measured outside the scatterer.[14] In general, an ISP can be a nonlinear problem and in our case nonlinearity between the polarizabilities of the elements and the sample points of the desired near-field pattern can be observed. This is due to the excitation of both *x*- and *y*-directed polarizations in a plasmonic particle. The array of plasmonic nanoparticles shapes the beam of the dipole source excitation located at the center. The dipole moments with general polarizations are induced on each element so that we have an array of dipoles where by tailoring the geometry of each element the required optical near-field concentration is established.

Choosing plasmonic particles as the array elements in our work is due to the fact that plasmonic materials have extreme

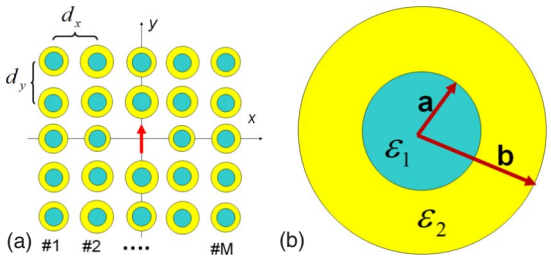

FIG. 1. (Color online) (a) Array of dielectric-plasmonic core-shell nanoparticles in $z=0$ plane. Excitation is an infinitesimal dipole located at the center and polarized along the y axis. (b) The geometry of spherical concentric dielectric-plasmonic core-shell nanoparticle.

interactions with the electromagnetic waves in optical regime. Designing and fabricating nanoantennas by using plasmonic particles have had a great development in recent years.[12,13,15–17] The frequency response of the amplitude of the polarizability of a plasmonic particle can possess a very high peak even though the size of the particle is very small in comparison with the wavelength.[11] The amplitude and phase of the polarizability have significant variations around the resonant frequency. Hence, for the concentric core-shell nanoplasmonic particle in which the core has a positive permittivity and the plasmonic shell has a negative permittivity, by changing (a/b) and (b/λ) wide-range amplitude and phase of the polarizability can be obtained. This property of the concentric core-shell nanoplasmonic particle is of great advantage when one uses it as an element in the array configuration.

II. FORMULATION: STEP-BY-STEP DESIGN PROCESS

Figure 1(a) depicts the configuration for an array of dielectric-plasmonic particles located at $z=0$ plane. The array has $N=M^2-1$ concentric elements, where M is the number of elements along the row and column in the geometry [shown in Fig. 1(a)]. The excitation is located at the center and is oriented along the y, which its performance must be shaped in the focal plane by using array elements. The unit-cell sizes along the x and y directions are considered to be d_x and d_y, respectively. Here, for the sake of simplicity a square unit cell with $d_x=d_y=d$ is assumed. The configuration of each element is depicted in Fig. 1(b). Each element is a concentric core-shell spherical particle with the inner and outer radius of a and b, respectively. The core is a dielectric material with positive permittivity ε_1 and the shell is made of a plasmonic material with negative and dispersive permittivity ε_2. The objective is to find the pair (a,b) for each element to engineer a desired pattern for y component of the electric field, $E_{y,des}$, at focal plane, $z=L$. This goal will be realized through an outlined step-by-step design process describing below. It is evident that any other component of the electric or magnetic field can also be tailored with the proper array of plasmonic particles. Notice that our problem can in fact be considered as an ISP in which the scattered field by the elements (or scatterers) is given in one plane (focal plane) and the geometry of the scatterers must be determined. During the design process, this ISP is turned out to be a nonlinear problem due to the coupled induced polarizations for the plasmonic nanoparticles.

The first step in the design approach is to obtain the dipolar mode equations, which is to find the x- and y-polarized electric dipole moments induced on each plasmonic element. Since the array elements have subwavelength sizes, from Mie theory, one can approximate the nth plasmonic particle with the electric dipole moment $\mathbf{p_n}$ and the polarizability α_n.[13,18] The dipole mode approximation is valid as long as the size of particles is small and further they are not in the near-touching zone where higher-order modes can be generated.[19,20] The design in our paper will be in the region that the electric dipole mode is sufficient to represent the physics[21,22] [the diameter of the particles $(2b)$ is less than 0.1λ and their surface to surface spacing is larger than $0.05b$]. Obviously, utilizing multipole expansion one can provide more accurate results when the distances between the particles are very small and in touching zone. This requires an extensive modeling and optimization. Here, a dipole mode approximation is used.

For the nth plasmonic element, one can then assume $\mathbf{p_n}=\alpha_n\mathbf{E_n}$, where $\mathbf{E_n}$ is the total electric field radiated by all other elements and the source. The vector dipolar mode equation can be expanded in two scalar equations as below

$$p_x^n = \alpha_n \left[\sum_{m=1,m\neq n}^{N} (G_{xx,z=0}^{nm} p_x^m + G_{xy,z=0}^{nm} p_y^m) + G_{xy,z=0}^{n0} p_{source} \right], \tag{1a}$$

$$p_y^n = \alpha_n \left[\sum_{m=1,m\neq n}^{N} (G_{yx,z=0}^{nm} p_x^m + G_{yy,z=0}^{nm} p_y^m) + G_{yy,z=0}^{n0} p_{source} \right]. \tag{1b}$$

In Eq. (1), p_x^n and p_y^n are x- and y-polarized electric dipole moments at the location of nth plasmonic element. For the dipole source at the center of the array, the electric dipole moment is $\mathbf{p_{source}}=\hat{\mathbf{y}}p_{source}$. The Green's function $G_{ws,z=0}^{nm}$, where $ws \in \{xx,xy,yx,yy\}$ is the electric field component in w direction at the location of nth element radiated by the unit electric dipole moment along s direction at the location of mth element. In other word, $G_{ws,z=0}^{nm}$ is the ws component of the electric dyadic Green's function (DGF), $\bar{\mathbf{G}}(\mathbf{r},\mathbf{r}')$, where $\mathbf{r}$ is the location of nth observation element and $\mathbf{r}'$ is the location of mth source element. A closed-form formula for the DGF is given as[23]

$$\bar{\mathbf{G}}(\mathbf{r},\mathbf{r}') = \frac{1}{4\pi\varepsilon_0}\frac{e^{-jk_0R}}{R^3}\left\{[(k_0R)^2 - jk_0R - 1]\bar{\mathbf{I}} - [(k_0R)^2 - j3k_0R - 3]\frac{\mathbf{RR}}{R^2}\right\}, \tag{2}$$

where $\bar{\mathbf{I}}$ is the identity dyad, $\mathbf{R}=\mathbf{r}-\mathbf{r}'$, $R=|\mathbf{R}|$, and $k_0=\omega\sqrt{\varepsilon_0\mu_0}$ is the free space wave number.

It must be mentioned that, for the array depicted in Fig. 1(a), there are no induced dipoles along the z direction for the plasmonic particles. The reason is explicable by using the

closed-form formula of DGF given in Eq. (2). As is observed, DGF includes two dyads: $\bar{\mathbf{I}}$ and $\mathbf{RR}$. Therefore, for the excitation which is along $\hat{\mathbf{y}}$, the radiated electric field at the source plane, $z=0$, has two components: one is parallel to $\bar{\mathbf{I}}.\hat{\mathbf{y}}=\hat{\mathbf{y}}$, and the other is parallel to $\mathbf{R}(\mathbf{R}.\hat{\mathbf{y}})$ or $\mathbf{R}$ vector. Since we have a planar array at $z=0$, $\mathbf{R}$ is in x-y plane and does not include any z component, that is why there is no z-polarized induced dipole. It is obvious that if there is an array of plasmonic particles over a curved surface, let us say a paraboloid or a sphere, then $\mathbf{R}$ can have all the components, and as a result all the x-, y-, and z-polarized induced dipoles may exist.

Equations (1a) and (1b) introduce $2N$ dipolar mode equations and one can recast a compact matrix form for them as follows:

$$\begin{bmatrix} [\mathbf{G}_{\mathbf{xx},\mathbf{z=0}}] & [\mathbf{G}_{\mathbf{xy},\mathbf{z=0}}] \\ [\mathbf{G}_{\mathbf{yx},\mathbf{z=0}}] & [\mathbf{G}_{\mathbf{yy},\mathbf{z=0}}] \end{bmatrix} \begin{bmatrix} [\mathbf{p}_\mathbf{x}] \\ [\mathbf{p}_\mathbf{y}] \end{bmatrix} = \begin{bmatrix} -[\mathbf{\Psi}_{\mathbf{x},\mathbf{z=0}}] \\ -[\mathbf{\Psi}_{\mathbf{y},\mathbf{z=0}}] \end{bmatrix}. \tag{3}$$

$[\mathbf{G}_{\mathbf{ws},\mathbf{z=0}}]$ is a $N\times N$ matrix, where its diagonal terms are related to the particles polarizabilities and its off-diagonal terms are obtained from the Green's functions $G^{nm}_{ws,z=0}$. The $N\times 1$ matrix $[\mathbf{p}_\mathbf{s}]$, $s\in\{x,y\}$, is defined with mth element equals to p^m_s. The source dipole effect is appeared in the right-hand side, in $N\times 1$ matrix $[\mathbf{\Psi}_{\mathbf{w},\mathbf{z=z_0}}]$, $w\in\{x,y\}$, which its nth element is $G^{n0}_{wy,z=0}p_{source}$. From Eqs. (1) and (3) one can readily obtain the below expressions for the diagonal terms of the $[\mathbf{G}_{\mathbf{ws},\mathbf{z=0}}]$ matrix

$$G^{nn}_{xx,z=0}=G^{nn}_{yy,z=0}=-\alpha_n^{-1}, \tag{4}$$

$$G^{nn}_{xy,z=0}=G^{nn}_{yx,z=0}=0. \tag{5}$$

Polarizabilities, α_n's and the matrix $[\mathbf{p}_\mathbf{s}]$ are the unknowns terms in Eq. (3), which are solved as below.

The second step in our design approach involves collocation (point-matching method) to relate the required x- and y-polarized dipoles, which satisfies Eq. (3), to the desired electric field pattern in the focal plane. As it was discussed earlier, the plasmonic-particles array is designed to provide the required two-dimensional narrow-beamwidth near-field pattern for a component of the electromagnetic fields, let us say E_y, at the focal plane $z=L$. Assuming one needs to achieve desired field pattern $f(x,y)$ as below

$$E_y(x,y,L)=f(x,y). \tag{6}$$

One needs N point-matching equations to obtain the required polarizablities. These required collocation equations are achieved by applying point matching on Eq. (6) at N points. These points are chosen to be the locations of plasmonic particles in the array. The obtained equation will be as below

$$f_n=\sum_{m=1}^{N}\left(G^{nm}_{yx,z=L}p^m_x+G^{nm}_{yy,z=L}p^m_y\right)+G^{n0}_{yy,z=L}p_{source}. \tag{7}$$

Here f_n is the value of the desired focusing function at the location of nth plasmonic element. In $G^{n,m}_{ws,z=L}$, the source point is at the location of the mth plasmonic element at $z=0$, and the observation point is at the focal plane, $z=L$, which its projection on $z=0$ is the location of the nth element. The compact form associated with the Eq. (7) is turned out to be

$$[[\mathbf{G}_{\mathbf{yx},\mathbf{z=L}}][\mathbf{G}_{\mathbf{yy},\mathbf{z=L}}]]\begin{bmatrix} [\mathbf{p}_\mathbf{x}] \\ [\mathbf{p}_\mathbf{y}] \end{bmatrix}=[\mathbf{f}]-[\mathbf{\Psi}_{\mathbf{y},\mathbf{z=L}}]. \tag{8}$$

$[\mathbf{f}]$ is constructed by f_n and the nth element of $[\mathbf{\Psi}_{\mathbf{y},\mathbf{z=L}}]$ includes the radiation of the central dipole which is equal to $G^{n0}_{yy,z=L}p_{source}$.

The third part of this design procedure is to set up an equation only in terms of the polarizabilities, α_n's. This equation can be achieved by eliminating the electric dipole moment matrices $[\mathbf{p}_\mathbf{x}]$ and $[\mathbf{p}_\mathbf{y}]$ from dipolar mode Eq. (3), and point matching Eq. (8), obtaining the below matrix equation

$$[[\mathbf{G}_{\mathbf{yx},\mathbf{z=L}}][\mathbf{G}_{\mathbf{yy},\mathbf{z=L}}]]\begin{bmatrix} [\mathbf{G}_{\mathbf{xx},\mathbf{z=0}}] & [\mathbf{G}_{\mathbf{xy},\mathbf{z=0}}] \\ [\mathbf{G}_{\mathbf{yx},\mathbf{z=0}}] & [\mathbf{G}_{\mathbf{yy},\mathbf{z=0}}] \end{bmatrix}^{-1}\begin{bmatrix} -[\mathbf{\Psi}_{\mathbf{x},\mathbf{z=0}}] \\ -[\mathbf{\Psi}_{\mathbf{y},\mathbf{z=0}}] \end{bmatrix} = [\mathbf{f}]-[\mathbf{\Psi}_{\mathbf{y},\mathbf{z=L}}]. \tag{9}$$

The recent equation is an inverse scattering equation, ISE because it relates the properties of the scattered field at $z=L$, $([\mathbf{f}]-[\mathbf{\Psi}_{\mathbf{y},\mathbf{z=L}}])$, to the scatterers, α_n's. In this ISE, the only unknowns are the diagonal components of $[\mathbf{G}_{\mathbf{xx},\mathbf{z=0}}]$ and $[\mathbf{G}_{\mathbf{yy},\mathbf{z=0}}]$, which are $-\alpha_n^{-1}$. It is of value to consider that the ISE given in Eq. (9) is a system of nonlinear equations in terms of α_n^{-1}. The inverse of the middle matrix creates the nonlinear effect. To solve this nonlinear matrix equation, there are several nonlinear solver techniques to be used.[24–26] Levenberg-Marquardt technique[26] has been found to be more appropriate for our study and will be applied here to successfully solve the nonlinear ISE given in Eq. (9). A discussion about this powerful approach for solving the nonlinear set of equations is presented in the Appendix.

The final step, fourth step, is to design the geometry of each concentric spherical particle which is finding the inner and outer radii a and b of each plasmonic particle, satisfying the obtained required polarizablities. As discussed earlier, by full analytical Mie scattering analysis,[27] the concentric core-shell particle depicted in Fig. 1(b) can be modeled by an induced electric dipole moment with the polarizability α. The higher-order terms are ignored considering the subwavelength sizes of the particles. As a result the polarizability which is the dipolar coupling between the electric field and the concentric core-shell particle is given as[11]

$$\alpha=\frac{-j6\pi\varepsilon_0}{k_0^3}\frac{U}{U-jV}, \tag{10}$$

where $e^{j\omega t}$ time convention is assumed throughout this paper and U is given by

TABLE I. Magnitude and phase of the induced dipoles along the y for the array of 5×5 nanoparticles. (a) $|p_y|$ (b) $\angle p_y$.

(a)

0.23	0.80	1.20	0.80	0.23
0.39	1.20	1.70	1.20	0.39
0.42	1.00	1.00	1.00	0.42
0.39	1.20	1.70	1.20	0.39
0.23	0.80	1.20	0.80	0.23

(b)

5.3	177.5	-2.3	177.5	5.3
5.0	178.3	-2.5	178.3	5.0
6.0	179.7	0	179.7	6.0
5.0	178.3	-2.5	178.3	5.0
5.3	177.5	-2.3	177.5	5.3

$$U=\begin{vmatrix} j_1(k_1a) & j_1(k_2a) & y_1(k_2a) & 0 \\ \tilde{j}_1(k_1a)/\varepsilon_1 & \tilde{j}_1(k_2a)/\varepsilon_2 & \tilde{y}_1(k_2a)/\varepsilon_2 & 0 \\ 0 & j_1(k_2b) & y_1(k_2b) & j_1(k_0b) \\ 0 & \tilde{j}_1(k_2b)/\varepsilon_2 & \tilde{y}_1(k_2b)/\varepsilon_2 & \tilde{j}_1(k_0b)/\varepsilon_0 \end{vmatrix}. \tag{11}$$

$j_1(x)$ and $y_1(x)$ are spherical Bessel functions of the first and second kind, respectively, and of the first order. Moreover $\tilde{z}(x)=d[xz(x)]/dx$, where z can be any of j_1 and y_1. Also k_1 and k_2 are the wave numbers of dielectric core and plasmonic shell, respectively. V is similar to U but in the fourth column in the determinant, $\tilde{j}_1$ and j_1 should be replaced by $\tilde{y}_1$ and y_1, correspondingly.

As mentioned before, the core is considered to be a dielectric material, and the shell a plasmonic material with Drude dispersive model as below[28]

$$\varepsilon_2=\varepsilon_0\left(1-\frac{\omega_p^2}{\omega(\omega-j\omega_D)}\right), \tag{12}$$

where ω_p and ω_D are the plasma and damping frequencies of the plasmonic material. Noble materials such as silver in optical regime can be used as the plasmonic shell for array elements. The numerical values for ω_p and ω_D can be achieved by fitting the experimental data of the noble metals' permittivity to the Drude model.[29] For example, at $\lambda=620$ nm, $\lambda=2\pi/k_0$, for $\omega_p=9.121\times10^{15}$ and $\omega_D=3.378\times10^{13}$ the permittivity of the shell will be $\varepsilon_2=\varepsilon_0(-8-j0.1)$.

After obtaining the magnitude and phase of polarizability ($|\alpha|$ and $\angle\alpha$) from Eq. (9), one can determine the inner and outer radii of the plasmonic particles, or equivalently the radii ratio a/b and normalized outer radius b/λ [by plotting $|\alpha|$ and $\angle\alpha$ using Eq. (10) in a plane constructed by the two independent variables a/b and b/λ and finding the intersection of these two contours]. The above methodology offers a successful design procedure to create the required plasmonic-array nanoparticles for a desired near-field manipulation, as will be highlighted for a typical example in the next section.

TABLE II. Magnitude and phase of the induced dipoles along the x for the array of 5×5 nanoparticles. (a) $|p_x|$ (b) $\angle p_x$.

(a)

0.06	0.16	0	0.16	0.06
0.09	0.11	0	0.09	0.11
0	0	0	0	0
0.11	0.09	0	0.09	0.11
0.06	0.16	0	0.16	0.06

(b)

-175.3	-7.8	0	172.2	4.7
178.6	177.0	0	-3.0	-1.4
0	0	0	0	0
-1.4	-3.0	0	177.0	178.6
4.7	172.2	0	-7.8	-175.3

TABLE III. Magnitude and phase of the polarizability of each of the core-shell nanoparticles for the 5×5 array. (a) $|\alpha|/\alpha_0$ (b) $\angle\alpha$ (in deg.).

(a)

0.053	0.060	0.063	0.060	0.053
0.054	0.058	0.067	0.058	0.054
0.054	0.044	↑	0.044	0.054
0.054	0.058	0.067	0.058	0.054
0.053	0.060	0.063	0.060	0.053

(b)

-1.5	-3.0	-2.2	-3.0	-1.5
-2.6	-2.3	-3.5	-2.3	-2.6
-1.9	-2.3	↑	-2.3	-1.9
-2.6	-2.3	-3.5	-2.3	-2.6
-1.5	-3.0	-2.2	-3.0	-1.5

III. PLASMONIC-PARTICLES CONCENTRATORS

In this section, the design procedure for an array of plasmonic particles engineering the near-field patterns in a specified focal plane is demonstrated. One needs to solve the nonlinear ISE equation given by Eq. (9) to achieve the required parameters. In all the cases studied in this section, the unit-cell size of $d=0.1\lambda$ is considered, and the focal length $L=0.15\lambda$ is assumed. Also, the desired pattern at $z=L$ is a two-dimensional sinc function [see Fig. 5(a)] with the null-to-null beamwidth of $\lambda/5$ given as below

$$f(x,y)=\frac{\sin(qx)}{qx}\frac{\sin(qy)}{qy}. \tag{13}$$

Here $q=5k_0$ is considered to obtain a $\lambda/5$ beamwidth. The resolution enhancement is defined as $R_e=q/k_0$ (=5).[7] The goal is to match the required near-field profile with the nulls of the sinc function and its peak value at the main beam. The permittivity of the core and shell for the elements are $\varepsilon_1=\varepsilon_0(2.2-j0.001)$ and $\varepsilon_2=\varepsilon_0(-8-j0.1)$ at the operational optical wavelength $\lambda=620$ nm (orange light in visible spectrum), respectively.

For the sake of simplicity and to demonstrate the physical meanings conveniently, we start with a 5×5 array of plasmonic particles. The objective is to determine the induced dipoles and the array elements configurations consequently.

TABLE IV. Geometry of each nanoparticle for the 5×5 array (a) b/λ (b) a/b.

(a)

0.044	0.049	0.043	0.049	0.044
0.045	0.048	0.049	0.048	0.045
0.045	0.040	↑	0.040	0.045
0.045	0.048	0.049	0.048	0.045
0.044	0.049	0.043	0.049	0.044

(b)

0.615	0.555	0.665	0.555	0.615
0.605	0.575	0.600	0.575	0.605
0.605	0.650	↑	0.650	0.605
0.605	0.575	0.600	0.575	0.605
0.615	0.555	0.665	0.555	0.615

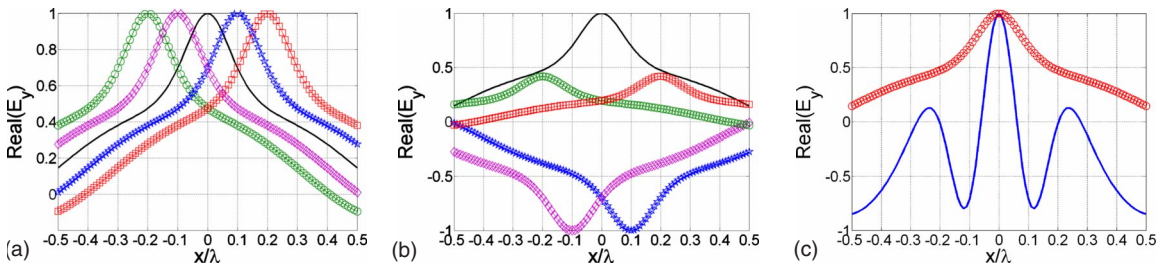

FIG. 2. (Color online) Focusing phenomenon for the real part of E_y in the focal plane ($z=0.15\lambda$). (a) Normalized shifted beams for the identical y-polarized infinitesimal dipoles located at $\mathbf{r}_{-2}=-0.2\lambda\hat{\mathbf{x}}$ (green with circle marker), $\mathbf{r}_{-1}=-0.1\lambda\hat{\mathbf{x}}$ (purple with diamond marker), $\mathbf{r}_0=\mathbf{0}$ (black with solid line), $\mathbf{r}_{+1}=0.1\lambda\hat{\mathbf{x}}$ (blue with pentagram marker), and $\mathbf{r}_{+2}=0.2\lambda\hat{\mathbf{x}}$ (red with square marker), (b) The shifted patterns multiplied by their weighting factors, $w_{\pm 2}=0.42\angle 6°$, $w_{\pm 1}=1\angle 179.7°$, and $w_0=1\angle 0°$, and (c) subwavelength beam which is the superposition of the five-weighted dipoles patterns (blue with solid line) and the pattern of a single dipole (red with circle marker).

To achieve this, we should follow the equations derived in Sec. II. Namely, for obtaining the desired pattern [Eq. (13)], one must first obtain the required p_x, p_y, α, and then the geometry configurations a and b for each element, as they are summarized in Tables I–IV. As obtained from (a) part of Tables I and II, the dominant polarization is p_y (since the source is polarized along the y). Another observation is the phase alternation of p_y between around 0° and 180° controlling the weighting functions for the field profile of each plasmonic particle, featuring the focusing phenomenon. To better understand this feature, in Fig. 2(a) we plot the field pattern for the y-polarized dipoles of the middle row in Table I when they have the same electric dipole moment. In Fig. 2(b) the performance of the dipoles with the proper weighting factors associated with the middle row in Table I is illustrated. Combination of these patterns will narrow the beam along the x axis as is shown in Fig. 2(c). In this figure we also show the performance of a single dipole for the sake of comparison and to highlight the success of our focusing approach.

The main challenge is next to create the dielectric-plasmonic core-shell nanoparticles array realizing the required induced dipoles. The advantage of considering core shells is the fact that one has more flexibility in the design space. For instance, in Fig. 3, we demonstrate $|\alpha|$ and $\angle\alpha$ in terms of b/λ and a/b which will be the design rule for achieving the required plasmonic particles. The magnitude of the polarizability $|\alpha|$ is normalized by a normalization factor $\alpha_0=4\pi\varepsilon_0/k_0^3$ for simplicity. A typical contour plot is shown in Fig. 4 that demonstrates how, for example, one can obtain the required core and shell radii, $(b/\lambda, a/b)=(0.043, 0.63)$, to achieve the required polarizability, $\alpha/\alpha_0=0.05\angle -3°$. The obtained α's ensure the required p_x and p_y manipulating the near-field pattern in the focal plane. It must be mentioned that not always one can achieve the exact required α. Therefore, one has to make an approximation in obtaining the required core-shell particle providing the best closest α in our design space. In this case, the phase of polarizability can be changed slightly to make the two contours have an intersection point in expense of suffering from some approximation. The accuracy of this procedure is highlighted well later in this section through the demonstrated results. Note that, the outer radius of each element should be less than the half of unit-cell size, i.e., $b<d/2$. In our case $d/(2\lambda)=0.050$ and in (a) part of Table IV, the constraint $b/\lambda<0.050$ is satisfied for all the plasmonic particles.

Let us now investigate the results for the design of a 5 $\times$5 plasmonic-particles array design. Figure 5(a) shows the required sinc function pattern in the focal plane and obviously our goal is to ensure the plasmonic particles can manipulate the near field in the focal plane as close as possible to the sinc function. The merit function is the nulls of the sinc (two at each side) and its peak at the main beam (since we have five spheres). Using more number of points can provide a better matching to the desired field profile (as will be investigated next). For the sake of comparison, the field pattern of a single dipole in the focal plane is also calculated in Fig. 5(b). The field performances for the array of induced dipoles and their approximated values (modeled by plasmonic nanoparticles) are plotted in Figs. 5(c) and 5(d), respectively. The approximated result refers to the case in which the phase of polarizability can be changed slightly to make the two polarizability phase and magnitude contours have an intersection point. As observed, our designed plasmonic particles can successfully engineer the near field in the required focal plane and enable the narrow-beam perfor-

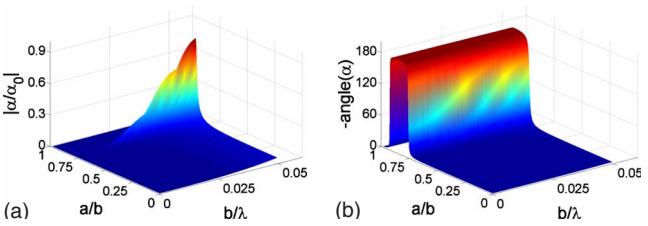

FIG. 3. (Color online) (a) Normalized amplitude of the polarizability, $|\alpha|/\alpha_0$ in terms of a/b and b/λ. (b) The phase performance, $-\angle\alpha$.

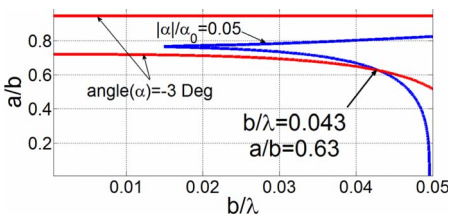

FIG. 4. (Color online) Design-rule curve for the geometry realization of the core-shell plasmonic particles, using polarizability magnitude and phase contours.

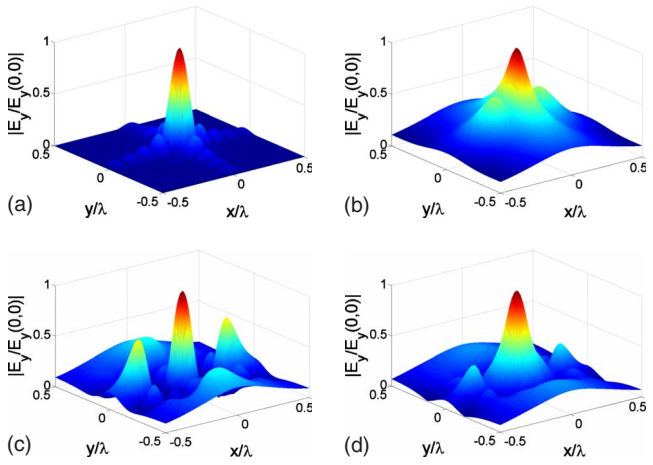

FIG. 5. (Color online) The magnitude of normalized E_y at the focal plane $z=0.15\lambda$ for (a) desired sinc function. (b) A single infinitesimal dipole. (c) Exact polarizabilities 5×5 array performance found by Levenberg-Marquardt technique, and (d) the approximated polarizabilities 5×5 array model.

mance. To demonstrate better the field performance of the array, the two-dimensional plots along the x and y axes are also demonstrated in Figs. 6(a) and 6(b), respectively. As observed from these figures, we are able to narrow the beam in both x and y directions with the use of our designed core-shell dielectric-plasmonic particles. The results derived for the exact induced dipole array successfully follow the nulls of the desired sinc function. The approximated core-shell dielectric-plasmonic particles performance is slightly deviated from the exact model result; however, still a narrow-beam characteristic is successfully developed.

To validate the accuracy of the proposed theoretical model, we apply a full-wave analysis based on CST commercial software to characterize the performance of the array of 5×5 dielectric-plasmonic core shells. The results are shown in Fig. 7 along the x and y directions. A good comparison is illustrated. The slight difference is due to the fact that in our modeling we approximate each nanoparticle with a dipole located at its center while in CST the whole spherical particle is modeled. Considering the near-field calculation, this slight difference is very much reasonable. A relatively good comparison is achieved, realizing beam focusing in the focal plane. Notice that in CST analysis the size of the dipole

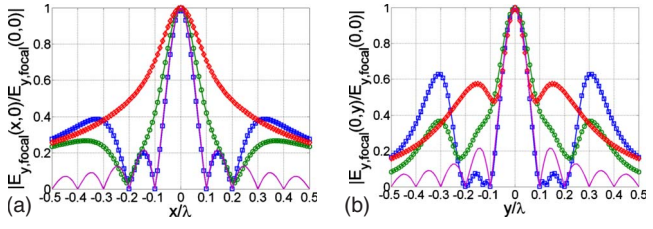

FIG. 6. (Color online) The magnitude of normalized E_y at the focal plane $z=0.15\lambda$ for the 5×5 array obtained by using the exact polarizabilities (blue with squarer marker), by using approximated polarizabilities (green with circle marker), for a single dipole along y at the origin (red with diamond marker), and for a desired sinc pattern (purple solid line). (a) Along x axis. (b) Along y axis.

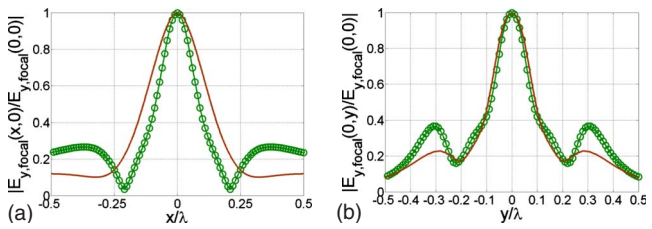

FIG. 7. (Color online) The magnitude of normalized E_y at the focal plane $z=0.15\lambda$ for the 5×5 array obtained based on our theoretical model (green with circle marker) and using full-wave CST simulation (brown solid line). (a) Along x axis. (b) Along y axis. A relatively good comparison is illustrated.

excitation is considered around 0.05λ (in the order of outer radius of the nanoparticles).

Increasing the number of array elements allows achieving a better near-field performance in regard of narrowing the beam. Figures 8(a) and 8(b) obtain the three-dimensional plots for the exact and approximated 11×11 polarizabilities designs, respectively. The successful beam narrowing is demonstrated. The two-dimensional plots are shown in Fig. 9. It is obtained that the 11×11 array design has a better characteristic than that of the 5×5 case (Fig. 6). One can see the null-to-null beamwidth for the 11×11 array along the x direction is about 0.36λ and along the y direction is about 0.2λ. The desired null-to-null beamwidth for both the x and y directions is 0.2λ. We need to mention that from all the obtained near fields in the focal plane, one can observe narrowing the beam along the y axis is more successful than along the x axis. This is because of having narrower beam for the dipole excitation itself along the y direction. Thus, there is more challenge to manipulate and focus the beam along the x direction. One solution to this will be if one uses more number of dielectric-plasmonic elements along the x direction so that the beam can be narrowed to our interest in this direction.

The concept and formulations developed in this paper allow successful optical near-field engineering with the use of array of plasmonic particles that can be uniform or nonuniform depending on the application of interest. Although a simple planar (rectangular) array is utilized here, where the elements are placed along a rectangular grid,[30] our formulation can be applied to other general arrays configurations enabling state-of-the-art optical applications. Other particles configurations such as multishells of different materials (increasing the design flexibility), and arrangements in unique

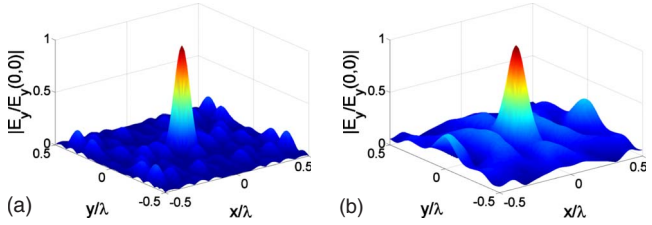

FIG. 8. (Color online) The magnitude of normalized E_y in the focal plane $z=0.15\lambda$ for the 11×11 array of plasmonic core-shell particles. (a) Exact polarizabilities array performance and (b) approximated polarizabilities model.

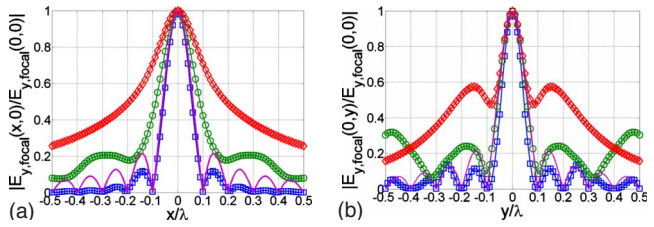

FIG. 9. (Color online) The magnitude of normalized E_y at the focal plane $z=0.15\lambda$ for the 11×11 array obtained by using the exact polarizabilities (blue with square marker), by using approximated polarizabilities (green with circle marker), for a single dipole along y at the origin (red with diamond marker) and for a desired sinc pattern (purple solid line) (a) along x axis and (b) along y axis. The 11×11 array can narrow the beam more successfully than the 5×5 case (obtained in Fig. 6).

patterns, can demonstrate desired physics. Further designs considering the fabrication realization are in progress.

IV. CONCLUSIONS

Array of dielectric-plasmonic core-shell nanoparticles is developed to engineer the near-field pattern and enable subwavelength optical focusing. Dipolar mode equations along with the dyadic Green's function formulation for the interaction between the elements are applied to summarize the required equations. Point-matching method is used and a nonlinear inverse scattering problem is determined to design the geometry of each array nanoparticle and establish the desired focusing pattern. Levenberg-Marquardt technique is successfully employed to solve the obtained set of nonlinear equations and find the polarizability of each element. The closed-form formula for the polarizability of a concentric core-shell nanoparticle is then employed to find the geometry configuration (the core and shell radii) for each element (with the use of magnitude and phase contours of the polarizability).

Arrays of 5×5 and 11×11 nanoparticles are developed to focus the optical beam in a specified focal plane, successfully. The physical meanings of the numerical results are highlighted. The subwavelength focusing is achieved by proper superposition of shifted beams in near field of each of the nanoparticles. Our theoretical model is compared well with a full-wave analysis based on the CST commercial software. Any component of the electromagnetic fields can be manipulated with the proper arrangements of the plasmonic nanoparticles. The proposed technique in this paper enables a capable approach for near-field engineering of the optical patterns with the use of novel array of plasmonic nanoparticles.

ACKNOWLEDGMENTS

This work is supported in part by the National Science Foundation (NSF) and the U.S. Air Force Office of Scientific Research (AFOSR). The authors would like to also thank the contribution of Soheil Saadat for helping to obtain the CST results.

APPENDIX

Levenberg-Marquardt algorithm,[26,31] LMA, is an elegant and heuristic method for solving simultaneous nonlinear equations. It is indeed a nonlinear least-squares algorithm. Let us assume that there is a set of N nonlinear equations with N unknowns which can be written as

$$\mathbf{F}(\mathbf{x}) = \mathbf{0}, \tag{A1}$$

where $\mathbf{F}=(F_1,F_2,F_3,\ldots,F_N)$ and $x=(x_1,x_2,x_3,\ldots,x_N)$. Instead of solving Eq. (A1) directly, the summation of the squares, $s(\mathbf{x})$, defined as below, will be minimized

$$s(\mathbf{x}) = \frac{1}{2}\sum_{n=1}^{N} F_n^2(\mathbf{x}). \tag{A2}$$

Hence, the efforts should be focused on obtaining the minimum of $s(\mathbf{x})$ which satisfies equation

$$\nabla s(\mathbf{x}) = \mathbf{0}. \tag{A3}$$

There are two common iterative algorithms for minimizing $s(\mathbf{x})$, gradient descent algorithm (GDA) and Gauss-Newton algorithm (GNA). As we illustrate in this appendix, LMA is just a blend of these two algorithms.

In GDA, which is actually the most intuitive technique to find the minima of a function, state update is performed by adding the negative scaled gradient at each step

$$\mathbf{x_{i+1}} = \mathbf{x_i} - \gamma_i \nabla s(\mathbf{x_i}), \tag{A4}$$

where $\gamma_i>0$ is the step size. When the gradient is small we would like to take large steps (large γ_i); conversely, small steps should be taken when the slope is not gentle (large gradient). The search direction $\mathbf{d_i}=-\gamma_i\nabla s(x_i)$ causes a convergent problem when the surface has a long and narrow valley. In this case, GDA is just rattling out the minima as the search direction is very small at the base of the valley and very large along the valley walls. To provide a successful LMA solver, the GDA's bottleneck and its advantage must be weighted properly (as will be seen later).

In GNA, the gradient of the function is expanded around the current state, $\mathbf{x_i}$, given by the Taylor series

$$\nabla s(\mathbf{x_{i+1}}) = \nabla s(\mathbf{x_i}) + [\mathbf{H}(\mathbf{x})]\,.\,(\mathbf{x_{i+1}} - \mathbf{x_i}) + \text{higher-order terms}, \tag{A5}$$

where $[\mathbf{H}(\mathbf{x})]$ is the Hessian matrix defined by

$$[\mathbf{H}(\mathbf{x})]_{m,n} = \frac{\partial^2 s}{\partial x_m\, \partial x_n}. \tag{A6}$$

As long as $s(\mathbf{x})$ has a quadratic behavior around the minima, higher-order terms of $(\mathbf{x_{i+1}}-\mathbf{x_i})$ can be neglected and the state update is found for GNA as

$$\mathbf{x_{i+1}} = \mathbf{x_i} - [\mathbf{H}(\mathbf{x_i})]^{-1}\,\nabla\, s(\mathbf{x_i}). \tag{A7}$$

A closed-form formula for Hessian can be obtained by taking a double gradient of Eq. (A2) as follows:

$$\nabla s(\mathbf{x}) = \sum_{n=1}^{N} F_n(\mathbf{x})\,\nabla\, F_n(\mathbf{x}) = [\mathbf{J}(\mathbf{x})]^T\mathbf{F}(\mathbf{x}), \tag{A8}$$

$$[\mathbf{H}(\mathbf{x})] = \nabla\nabla s(\mathbf{x}) = [\mathbf{J}(\mathbf{x})]^T[\mathbf{J}(\mathbf{x})] + \sum_{n=1}^{N} F_n(\mathbf{x})\,\nabla\,\nabla F_n(\mathbf{x}), \tag{A9}$$

where $[\mathbf{J}(\mathbf{x})]$ is the Jacobian defined as $[\mathbf{J}(\mathbf{x})]_{m,n} = \partial F_m / \partial x_n$. According to Eq. (A1), it is possible to assume each nonlinear function, $F_m(\mathbf{x})$, small near the solution so that an approximation for Hessian can be determined as given below

$$[\mathbf{H}(\mathbf{x})] = [\mathbf{J}(\mathbf{x})]^T[\mathbf{J}(\mathbf{x})]. \tag{A10}$$

When around the minima $s(\mathbf{x})$ has a quadratic behavior, GNA converges rapidly. So GNA and GDA are complementary in the advantages they provide. Levenberg proposed an algorithm whose update rule is a blend of GNA and GDA which is given by

$$\mathbf{x_{i+1}} = \mathbf{x_i} - ([\mathbf{H}(\mathbf{x_i})] + \gamma_i[\mathbf{I}])^{-1}\,\nabla\, s(\mathbf{x_i}), \tag{A11}$$

where $[\mathbf{I}]$ is the identity matrix. Following an update, if the error is reduced, it implies that the quadratic assumption on $s(\mathbf{x})$ is working and we reduce γ_i (usually by a factor of 10) to reduce the influence of GDA. On the other hand, if the error is increased, GDA is more prior to be followed; and hence γ_i is increased by the same factor.

When the value of γ_i is large, larger movement should be taken along the directions where the curvature is low, this crucial insight was provided by Marquardt. Since the diagonal terms of the Hessian are proportional to the curvature of $s(\mathbf{x})$, Marquardt replaced the identity matrix in Eq. (A10) with the diagonal terms of Hessian, resulting to the well-known Levenberg-Marquardt update rule [after we replace the gradient by Eq. (A8)].

$$\mathbf{x_{i+1}} = \mathbf{x_i} - ([\mathbf{H}(\mathbf{x_i})] + \gamma_i\,\mathrm{diag}[\mathbf{H}(\mathbf{x_i})])^{-1}\,.\,[\mathbf{J}(\mathbf{x})]^T\mathbf{F}(\mathbf{x}). \tag{A12}$$

LMA works extremely well in practice and has become the standard of nonlinear least-squares solvers.

*rashiditarha.a@neu.edu
†hosseinm@ece.neu.edu

[1] R. F. Oulton, V. J. Sorger, T. Zentgraf, R. Ma, C. Gladden, L. Dai, G. Bartal, and X. Zhang, Nature (London) **461**, 629 (2009).
[2] T. L. Andrew, H. Tsai, and R. Menon, Science **324**, 917 (2009).
[3] A. Grbic and G. V. Eleftheriades, Phys. Rev. Lett. **92**, 117403 (2004).
[4] E. A. Ash and G. Nicholls, Nature (London) **237**, 510 (1972).
[5] J. B. Pendry, Phys. Rev. Lett. **85**, 3966 (2000).
[6] A. Grbic and G. V. Eleftheriades, Appl. Phys. Lett. **82**, 1815 (2003).
[7] A. Grbic and R. Merlin, IEEE Trans. Antennas Propag. **56**, 3159 (2008).
[8] R. Merlin, Science **317**, 927 (2007).
[9] M. F. Imani and A. Grbic, IEEE Antennas Wireless Propag. Lett. **8**, 421 (2009).
[10] L. Markley, A. M. H. Wong, Y. Wang, and G. V. Eleftheriades, Phys. Rev. Lett. **101**, 113901 (2008).
[11] J. Li, A. Salandrino, and N. Engheta, Phys. Rev. B **76**, 245403 (2007).
[12] S. Ghadarghadr, Z. Hao, and H. Mosallaei, Opt. Express **17**, 18556 (2009).
[13] A. Ahmadi, S. Ghadarghadr, and H. Mosallaei, Opt. Express **18**, 123 (2010).
[14] W. C. Chew, *Waves and Fields in Inhomogeneous Media*, 2nd ed. (IEEE Press, New York, 1995).
[15] J. Li and N. Engheta, IEEE Trans. Antennas Propag. **55**, 3018 (2007).
[16] P. Muhlschlegel, H.-J. Eisler, O. J. F. Martin, B. Hecht, and D. W. Pohl, Science **308**, 1607 (2005).
[17] J. K. Gansel, M. Thiel, M. S. Rill, M. Decker, K. Bade, V. Saile, G. V. Freymann, S. Linden, and M. Wegener, Science **325**, 1513 (2009).
[18] A. Alù and N. Engheta, Phys. Rev. B **75**, 024304 (2007).
[19] S. Y. Park and D. Stroud, Phys. Rev. B **69**, 125418 (2004).
[20] I. Romero, J. Aizpurua, G. W. Bryant, and F. J. G. de Abajo, Opt. Express **14**, 9988 (2006).
[21] S. Ghadarghadr and H. Mosallaei, IEEE Trans. Antennas Propag. **57**, 149 (2009).
[22] S. Ghadarghadr and H. Mosallaei, IEEE Trans. NanoTechnol. **8**, 582 (2009).
[23] H. C. Chen, *Theory of Electromagnetic Waves: A Coordinate-Free Approach* (McGraw-Hill, New York, 1983).
[24] W. H. Press, S. A. Teukolsky, W. T. Vetterling, and B. P. Flannery, *Numerical Recipes in Fortran 77: The Art of Scientific Computing*, 2nd ed. (Cambridge University Press, New York, 2006), Vol. 1.
[25] A. R. Conn, N. I. M. Gould, and P. L. Toint, *Trust-Region Methods*, MPS/SIAM Series on Optimization (SIAM and MPS, Philadelphia, 2000).
[26] D. Marquardt, SIAM J. Appl. Math. **11**, 431 (1963).
[27] A. Alù and N. Engheta, J. Appl. Phys. **97**, 094310 (2005).
[28] N. Engheta and R. W. Ziolkowski, *Metamaterials: Physics and Engineering* (Wiley, New York, 2006).
[29] P. B. Johnson and R. W. Christy, Phys. Rev. B **6**, 4370 (1972).
[30] C. A. Balanis, *Antenna Theory: Analysis and Design*, 3rd ed. (Wiley, New York, 2005).
[31] A. Ranganathan, private communication for his work on "The Levenberg-Marquardt Algorithm" available on http://ananth.in/docs/lmtut.pdf, 2004.